

Supplementary information

Dual-Supramolecular Contacts Induce Extreme Hofmann Framework Distortion and Multi-Stepped Spin-Crossover

Manan Ahmed,^a Helen E. A. Brand,^b Vanessa K. Peterson,^c Jack K. Clegg,^d Cameron J. Kepert,^e Jason R. Price,^{a,b} Benjamin J. Powell^f and Suzanne M. Neville ^{*a}

^a School of Chemistry, The University of New South Wales, Sydney, 2052 Australia. *Email: s.neville@unsw.edu.au

^b The Australian Synchrotron, 800 Blackburn Road, Clayton, Victoria, Australia.

^c ANSTO, Lucas Heights, New South Wales, Australia.

^d School of Chemistry and Molecular Biosciences, The University of Queensland, St Lucia, Queensland 4072, Australia.

^e The School of Chemistry, The University of Sydney, Sydney, 2006 Australia.

^f School of Mathematics and Physics, The University of Queensland, St Lucia, Queensland 4072, Australia.

Contents

- S1. Thermogravimetric analysis (TGA)
- S2. Single crystal X-ray diffraction
- S3. Magnetic susceptibility
- S4. Differential scanning calorimetry (DSC)
- S5. Hirshfeld surface analysis
- S6. Powder diffraction

S1. Thermogravimetric analysis (TGA)

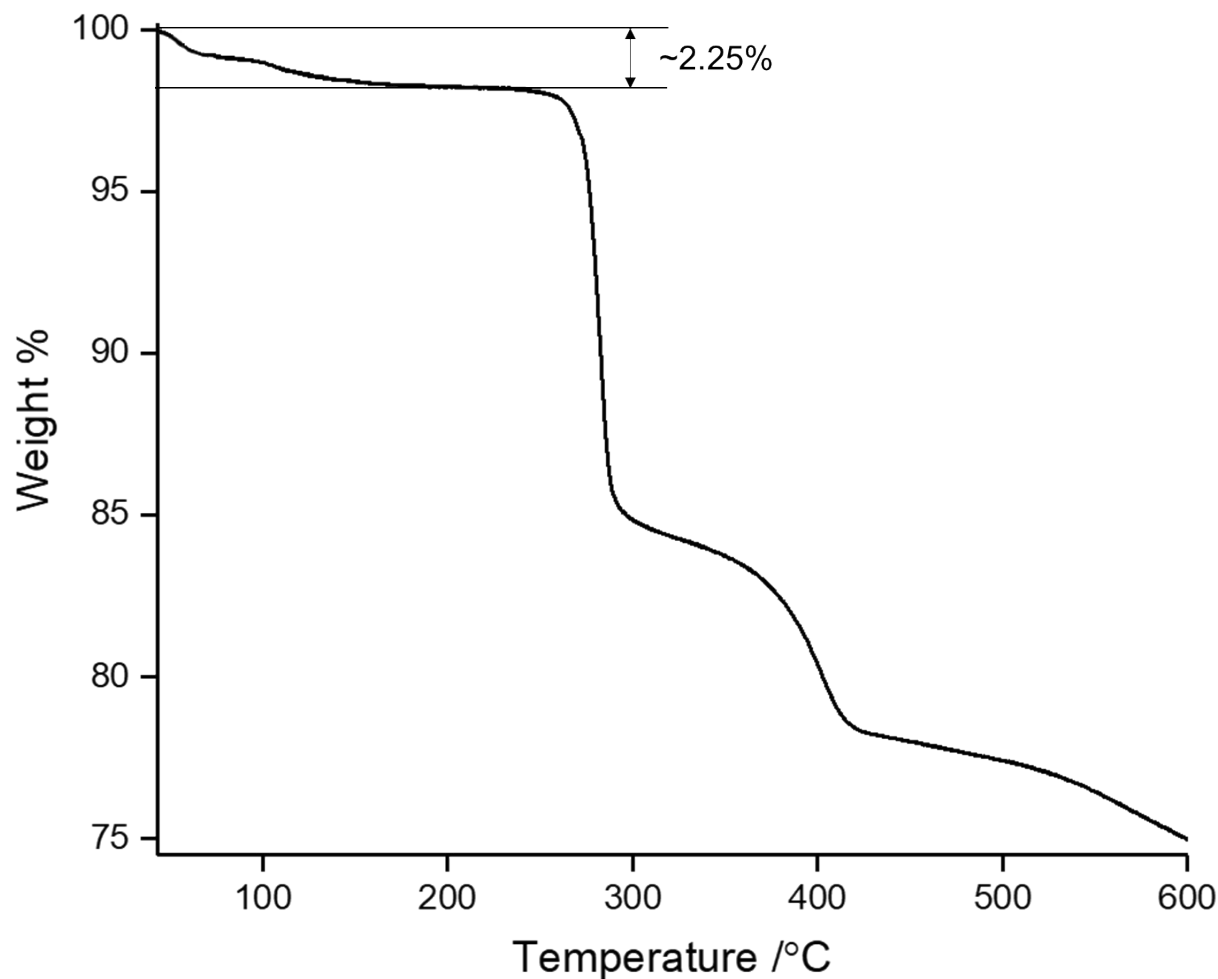


Figure S1. Thermogravimetric analysis of $[\text{Fe}_3(\text{N-cintrz})_6(\text{Pd}(\text{CN})_4)_3] \cdot 6\text{H}_2\text{O}$ showing the solvent loss in two steps with an overall loss of $\sim 2.25\%$ (*cf.* theoretical 2.39 %) up to 150 °C. Beyond 150 °C the framework decomposes.

S2. Single crystal X-ray diffraction

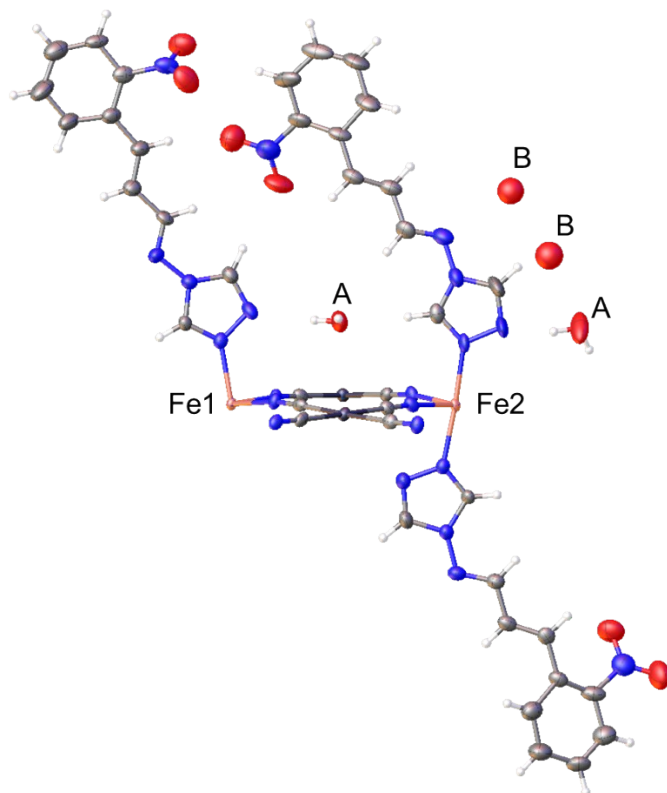


Figure S2. Asymmetric unit of $[Fe_3(N\text{-cintrz})_6(Pd(CN)_4)_3] \cdot 6H_2O$ at 150 K

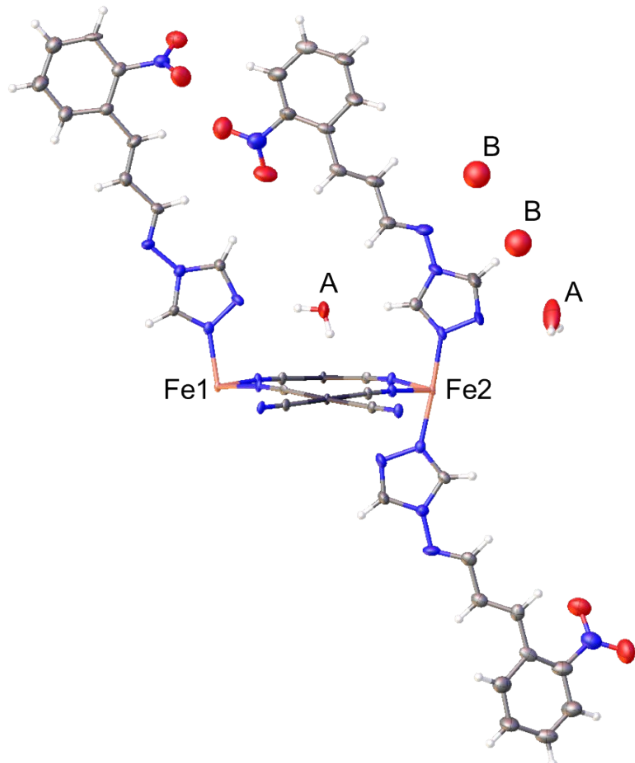


Figure S3. Asymmetric unit of $[Fe_3(N\text{-cintrz})_6(Pd(CN)_4)_3] \cdot 6H_2O$ at 100 K

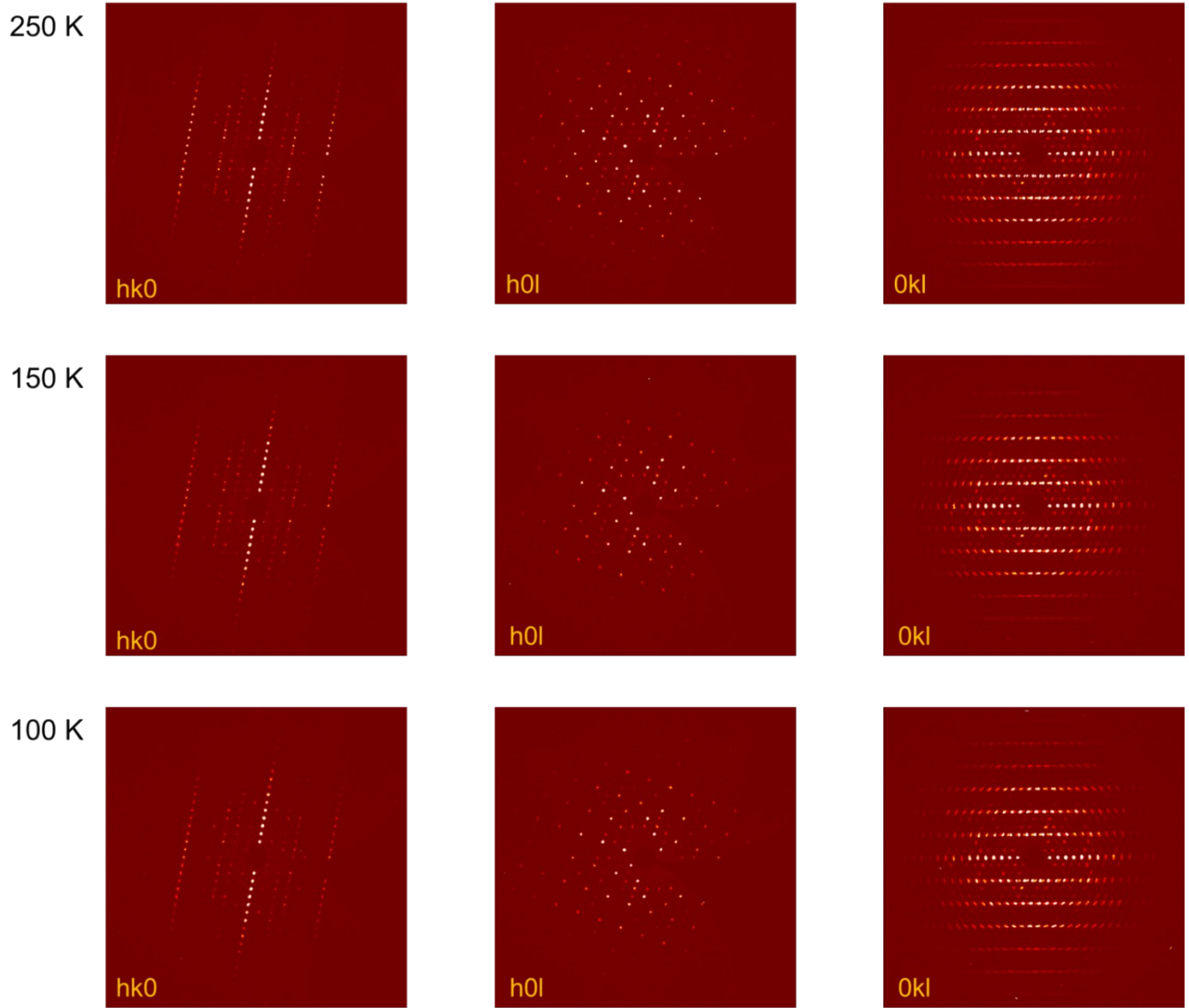


Figure S4. Precession images of $[\text{Fe}_3(\text{N}-\text{cintrz})_6(\text{Pd}(\text{CN})_4)_3] \cdot 6\text{H}_2\text{O}$ generated from single crystal X-ray diffraction data.

Table S1. Crystallographic data and refinement parameters for $[\text{Fe}_3(\text{N}-\text{cintrz})_6(\text{Pd}(\text{CN})_4)_3] \cdot 6\text{H}_2\text{O}$

Parameters			
Empirical formula	$\text{C}_{78}\text{H}_{62}\text{Fe}_3\text{N}_{42}\text{O}_{18}\text{Pd}_3$		
Formula weight g/mol	2362.44		
T/ K	250	150	100
Crystal system	Triclinic		
Space group	$P-1$		
$a / \text{\AA}$	10.5134(8)	10.3089(12)	10.1602(9)
$b / \text{\AA}$	15.8864(15)	15.7917(19)	15.7199(15)
$c / \text{\AA}$	16.5425(15)	16.1627(18)	15.9084(14)
$\alpha / {}^\circ$	110.227(4)	110.114(4)	110.052(3)
$\beta / {}^\circ$	107.844(3)	107.329(4)	106.996(3)
$\gamma / {}^\circ$	92.631(3)	93.312(5)	93.533(4)
Volume / \AA^3	2431.9(4)	2320.61(5)	2245.23(4)
Z	1		
$\rho_{\text{calc}} \text{ g/cm}^3$	1.613	1.690	1.747
F(000)	1184	1184	1184
μ / mm^{-1}	1.065	1.116	1.153
$\theta \text{ min-max/}{}^\circ$	2.057-27.513	2.103-27.581	2.131-27.578
Crystal size / mm^3	$0.152 \times 0.75 \times 0.025$		
Data/restraints/parameters	11169, 0, 664	10288, 0, 664	9976, 0, 664
Goodness-of-fit on F^2	1.023	1.052	1.067
$R_1 [I > 2\sigma(I), \text{ all data}]$	0.0641, 0.0880	0.0689, 0.1180	0.0638, 0.0996
wR ₂ [$I > 2\sigma(I)$, all data]	0.1854, 0.2029	0.1762, 0.1995	0.1479, 0.1633

Table S2: Selected structure parameters for $[\text{Fe}_3(\text{N}-\text{cintrz})_6(\text{Pd}(\text{CN})_4)_3] \cdot 6\text{H}_2\text{O}$

Selected parameters	Temperature /K		
	250	150	100
Fe \cdots Fe /Å	7.414	7.297	7.221
Fe1 C≡N /°	169.5- 174.3	170.9- 174.7	172.4- 175.2
Fe2 C≡N /°	168.9- 173.5	170.5- 174.2	171.2- 175.5
Fe2-N-N ^{trz} _{L1} /°	91.56	91.90	92.40
Fe2-N-N ^{trz} _{L2} /°	86.99	87.10	86.86
Fe1-N-N ^{trz} _{L3} /°	92.07	92.30	92.11
Interlayer distance /Å	15.24	15.10	15.01
Torsion angle /°			
L1 (N11-N10-C26-N14)	172.1	171.4	171.9
L2 (N16-N15-C33-N19)	152.0	152.7	152.3
L3 (N3-N4-C13-N7)	169.2	169.1	169.4

Table S3. Hydrogen bonds for $[\text{Fe}_3(\text{N}-\text{cintrz})_6(\text{Pd}(\text{CN})_4)_3] \cdot 6\text{H}_2\text{O}$

Donor...Acceptor (\AA)	Temperature		
	250 K	150 K	100 K
Host···host			
L1···L3			
O2···C7	3.068	3.032	3.011
O3···C7	3.253	3.191	3.183
O3···C5	3.395	3.469	3.539
O4···C4	3.404	3.412	3.466
L1···L2			
O6···C20	3.298	3.363	3.452
N6···C27	3.450	3.418	3.411
Guest···host			
O7W···N4	2.992	2.941	2.914
O7W···C16	3.302	3.203	3.166
O8W···N11	2.764	2.744	2.722

S3. Magnetic susceptibility

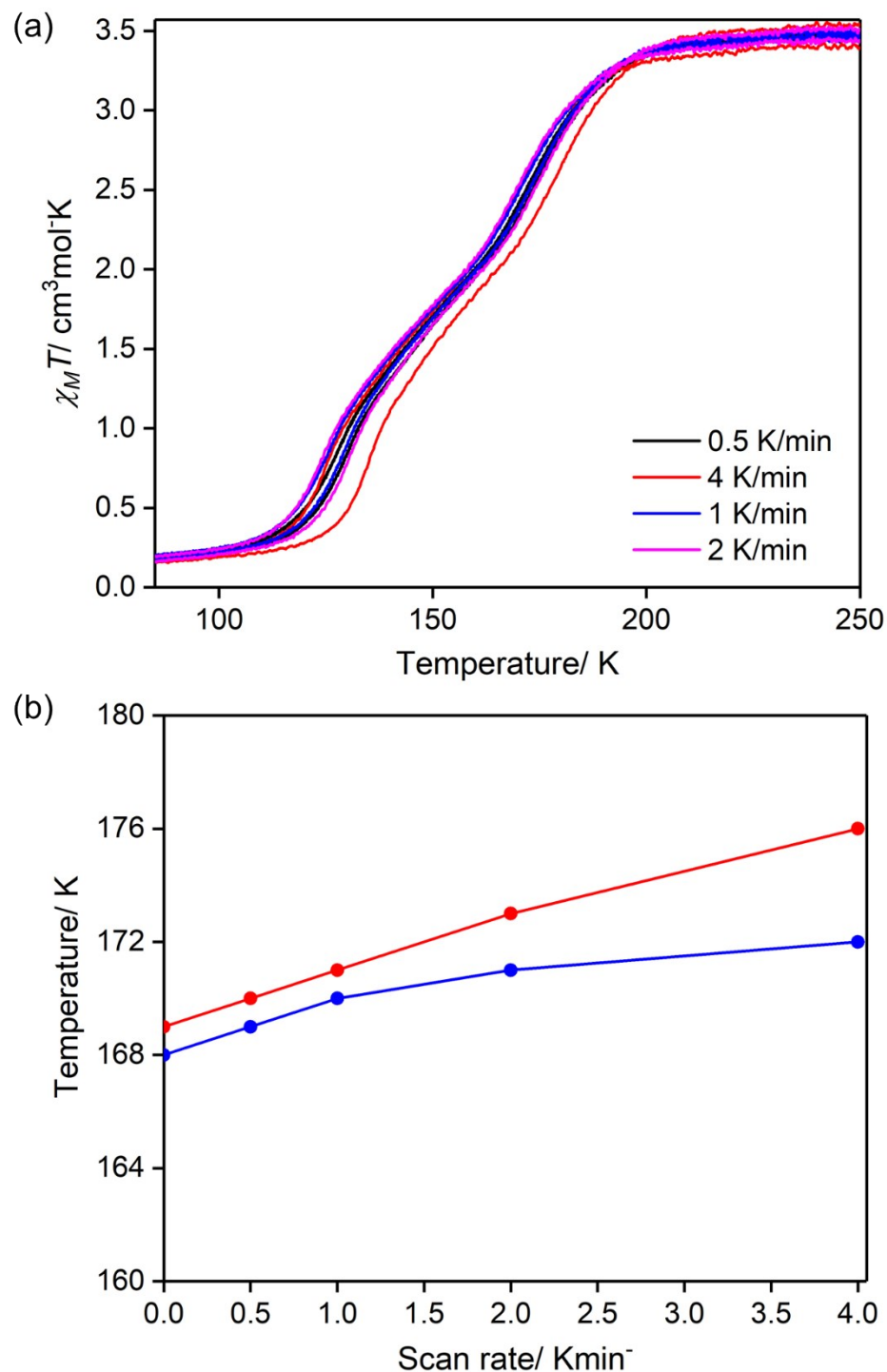


Figure S5. (a) Variable scan rate magnetic susceptibility of $[\text{Fe}_3(\text{N}-\text{cintrz})_6(\text{Pd}(\text{CN})_4)_3] \cdot 6\text{H}_2\text{O}$ (0.5, 4, 1 and 2 K/min) (b) Scan rate vs $T_{1/2}$ plot ($T_{1/2} \downarrow$: blue and $T_{1/2} \uparrow$: red; at rate = 0 Kmin^{-1} $T_{1/2} \downarrow$: 168, 169 K).

S4. Differential scanning calorimetry (DSC)

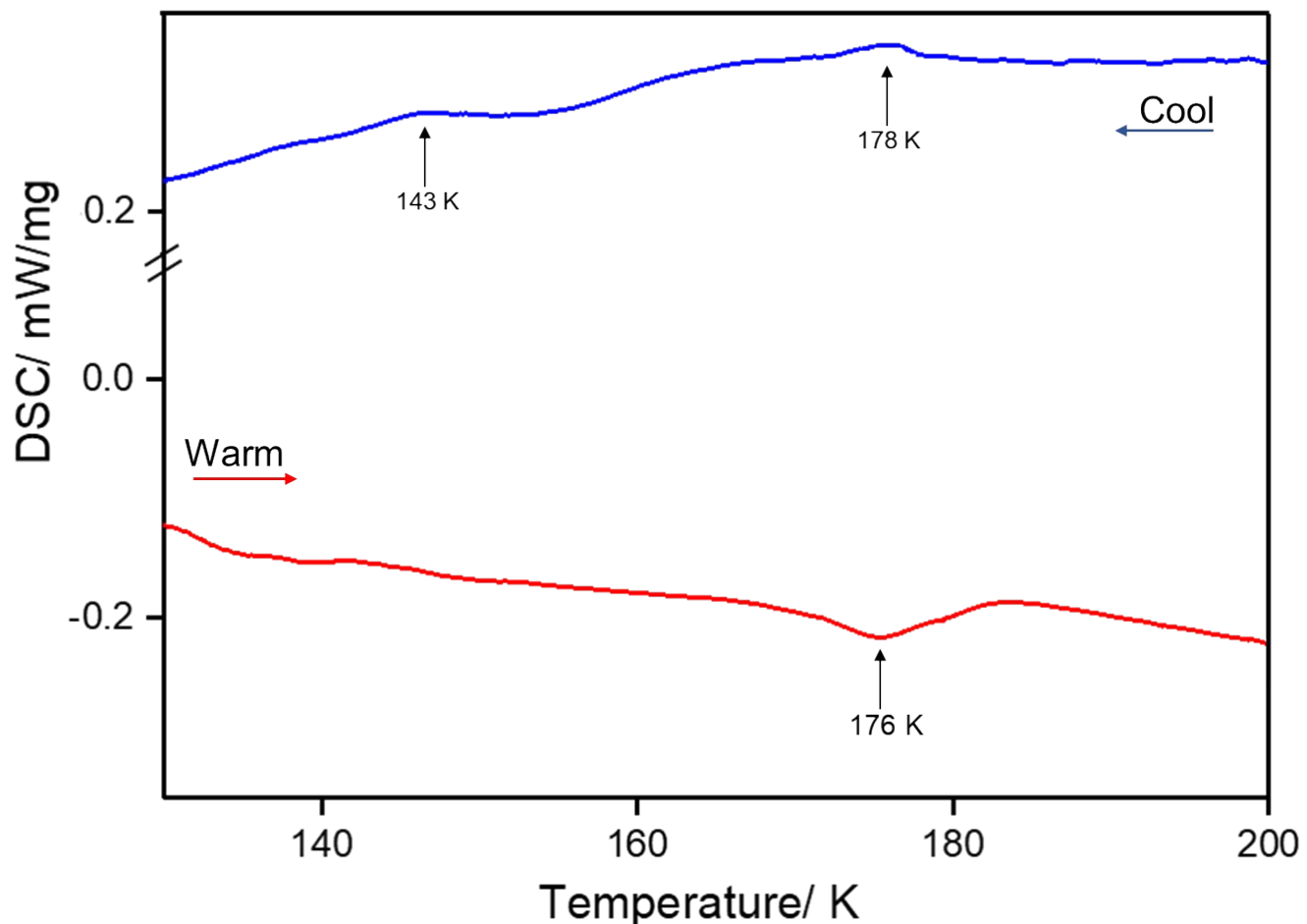


Figure S6: DSC measurement curve of $[Fe_3(N\text{-cintrz})_6(Pd(CN)_4)_3] \cdot 6H_2O$ at the scan rate of 10 K/min, demonstrating a two-step spin transition.

S5. Hirshfeld surface analysis

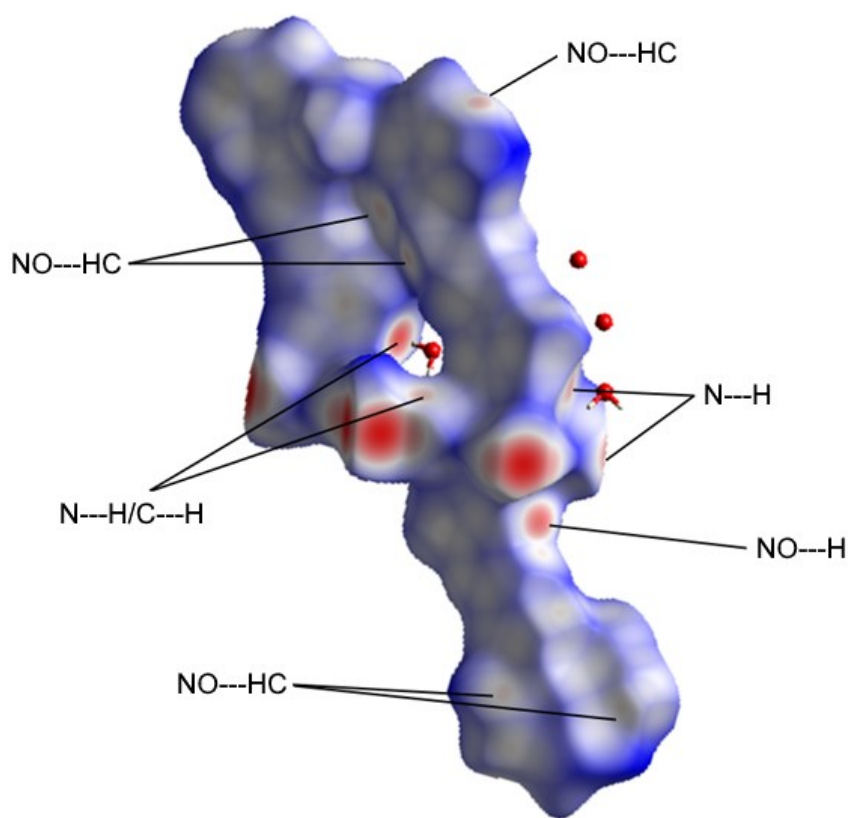


Figure S7. Hirshfeld 3-D plot at 250 K, large red spots indicate the covalent bond interaction and small red spot indicates the $\text{NO}\cdots\text{N}$, $\text{N}\cdots\text{H}$ and $\text{C}\cdots\text{H}$ interactions.

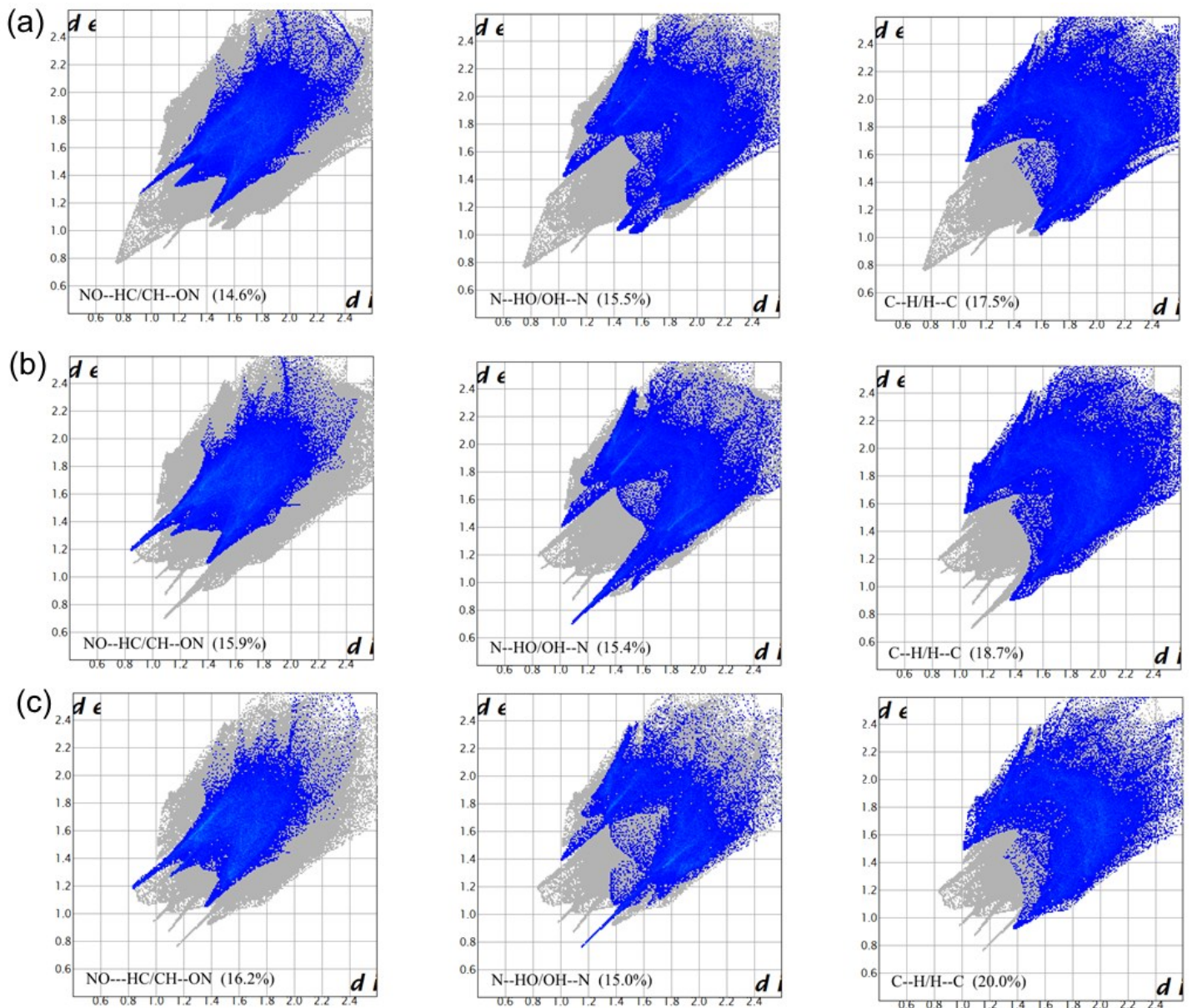


Figure S8: Hirshfeld 2-D fingerprint plot of $[\text{Fe}_3(\text{N}-\text{cintrz})_6(\text{Pd}(\text{CN})_4)_3] \cdot 6\text{H}_2\text{O}$ showing $\text{NO}\cdots\text{HC}$, $\text{N}\cdots\text{HO}$ and $\text{C}\cdots\text{H}$ intermolecular interactions at (a) 250 K (b) 150 K (c) 100 K.

S6. Powder diffraction

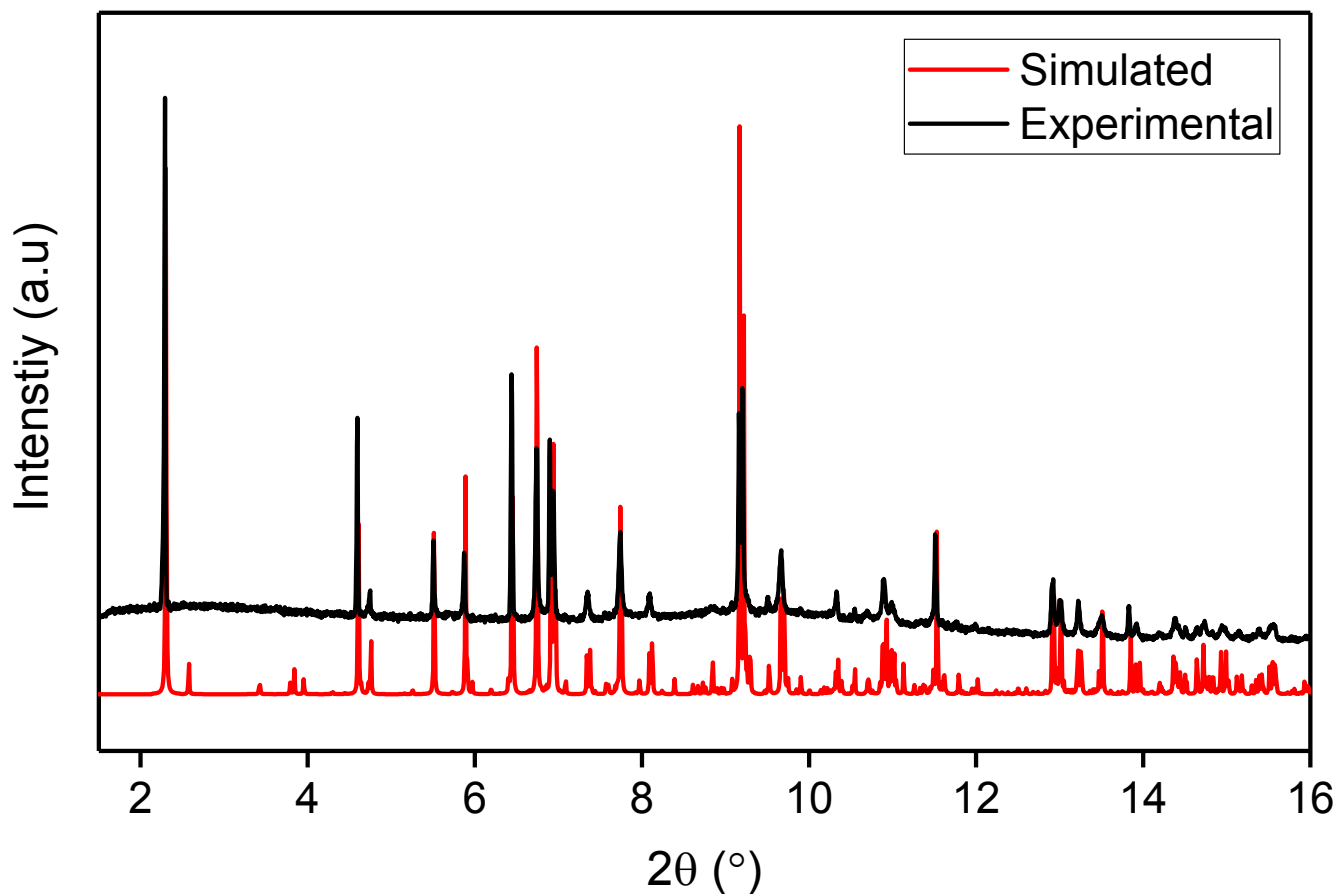


Figure S9. Comparison of powder diffraction data with that simulated from the single crystal diffraction data reveal the phase purity of $[\text{Fe}_3(\text{N}-\text{cintrz})_6(\text{Pd}(\text{CN})_4)_3] \cdot 6\text{H}_2\text{O}$ at 250 K ($\lambda = 0.59033 \text{ \AA}$).

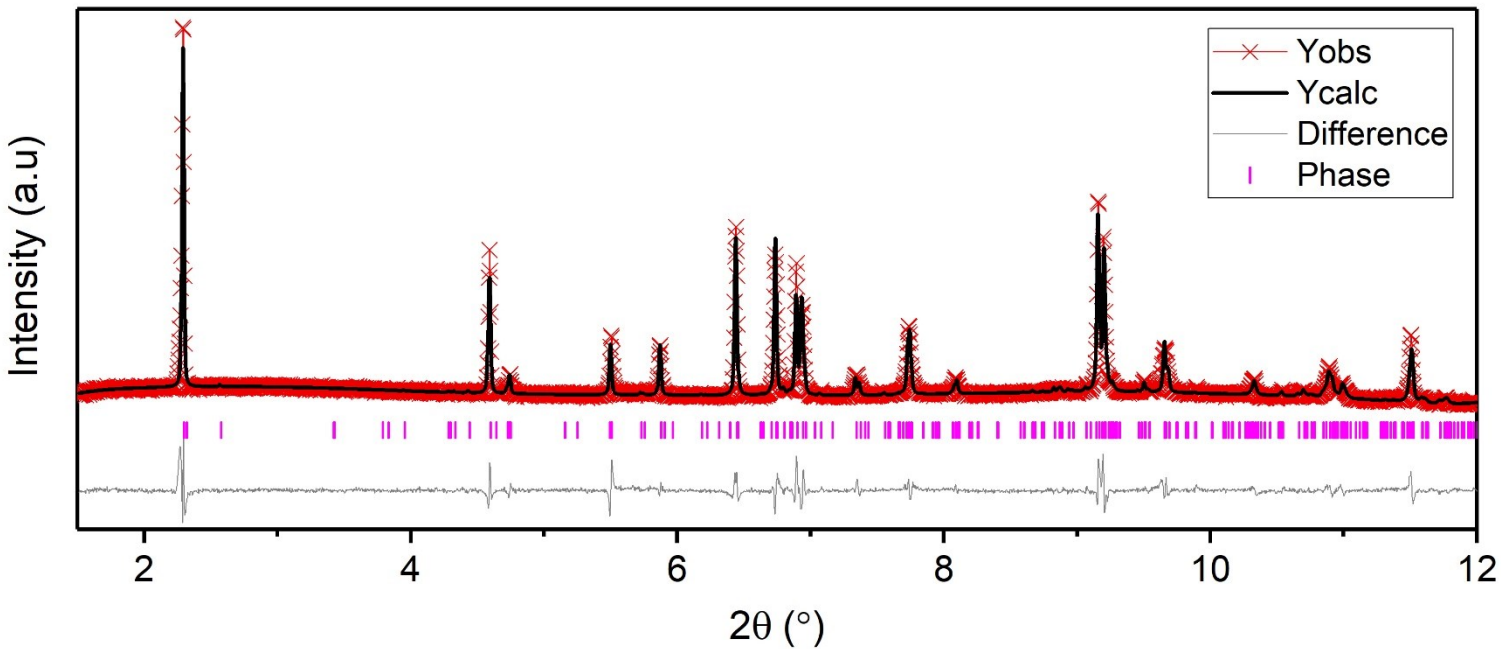


Figure S10. Le Bail refinement of PXRD pattern of $[\text{Fe}_3(\text{N}-\text{cintrz})_6(\text{Pd}(\text{CN})_4)_3] \cdot 6\text{H}_2\text{O}$ at 250 K. Refined parameters: $a = 10.254 \text{ \AA}$, $b = 15.265 \text{ \AA}$ and $c = 16.254 \text{ \AA}$, $\alpha = 110.163^\circ$, $\beta = 107.665^\circ$, $\gamma = 92.688^\circ$, $V = 2434.32 \text{ \AA}^3$ (*cf.* single crystal at 250 K: $a = 10.513$, $b = 15.886$, $c = 16.542$, $\alpha = 110.227^\circ$, $\beta = 107.84^\circ$, $\gamma = 92.631^\circ$, $V = 2431.90 \text{ \AA}^3$).

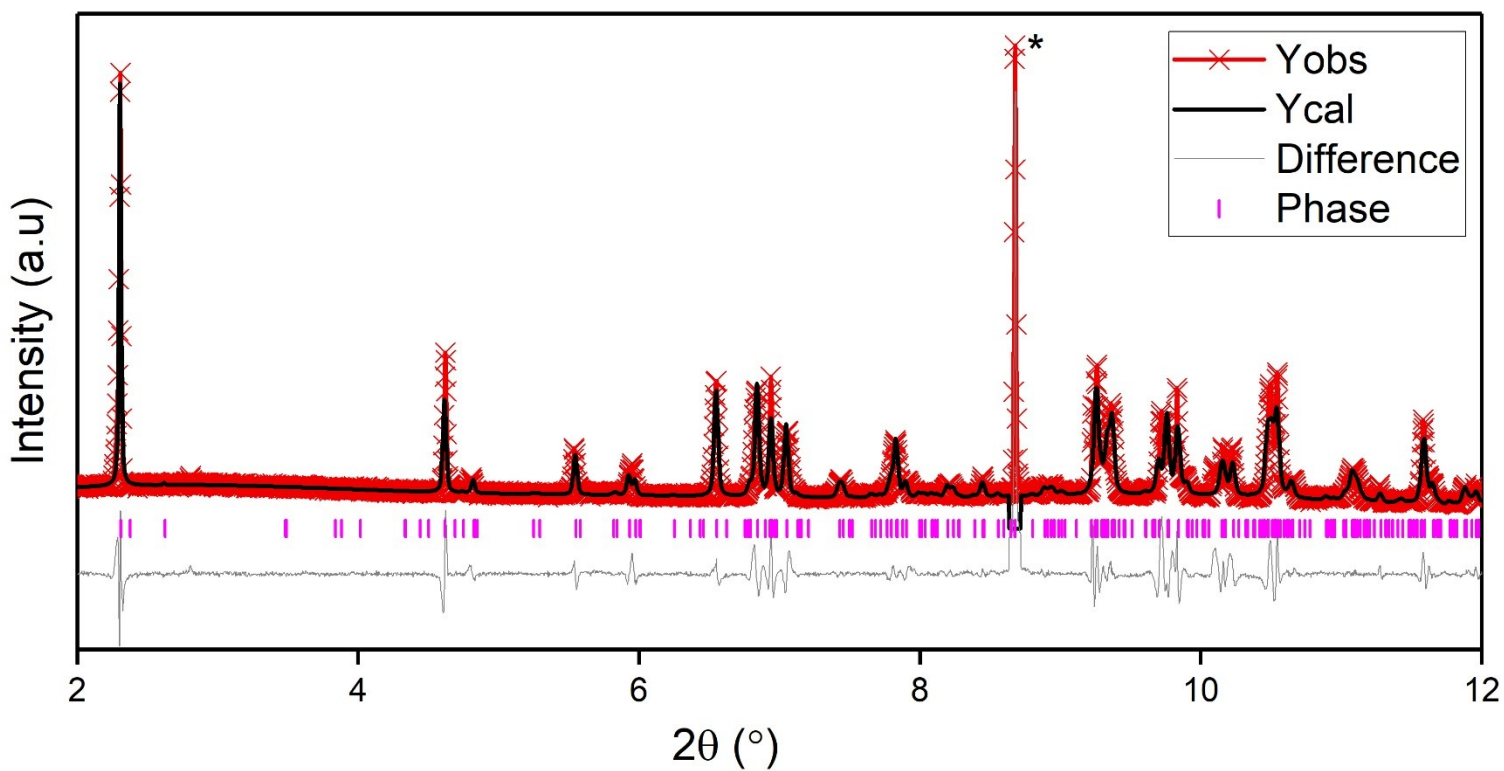


Figure S11. Le Bail refinement of PXRD pattern of $[\text{Fe}_3(\text{N}-\text{cintrz})_6(\text{Pd}(\text{CN})_4)_3] \cdot 6\text{H}_2\text{O}$ at 150 K. Refined parameters: $a = 10.338 \text{ \AA}$, $b = 15.801 \text{ \AA}$ and $c = 16.117 \text{ \AA}$, $\alpha = 109.880^\circ$, $\beta = 107.387^\circ$, $\gamma = 92.788^\circ$, $V = 2323.2 \text{ \AA}^3$ (*cf.* single crystal at 150 K: $a = 10.308$, $b = 15.791$, $c = 16.162$, $\alpha = 110.114^\circ$, $\beta = 107.329^\circ$, $\gamma = 93.312^\circ$, $V = 2320.6 \text{ \AA}^3$). * mark indicates the solvent freezing peak

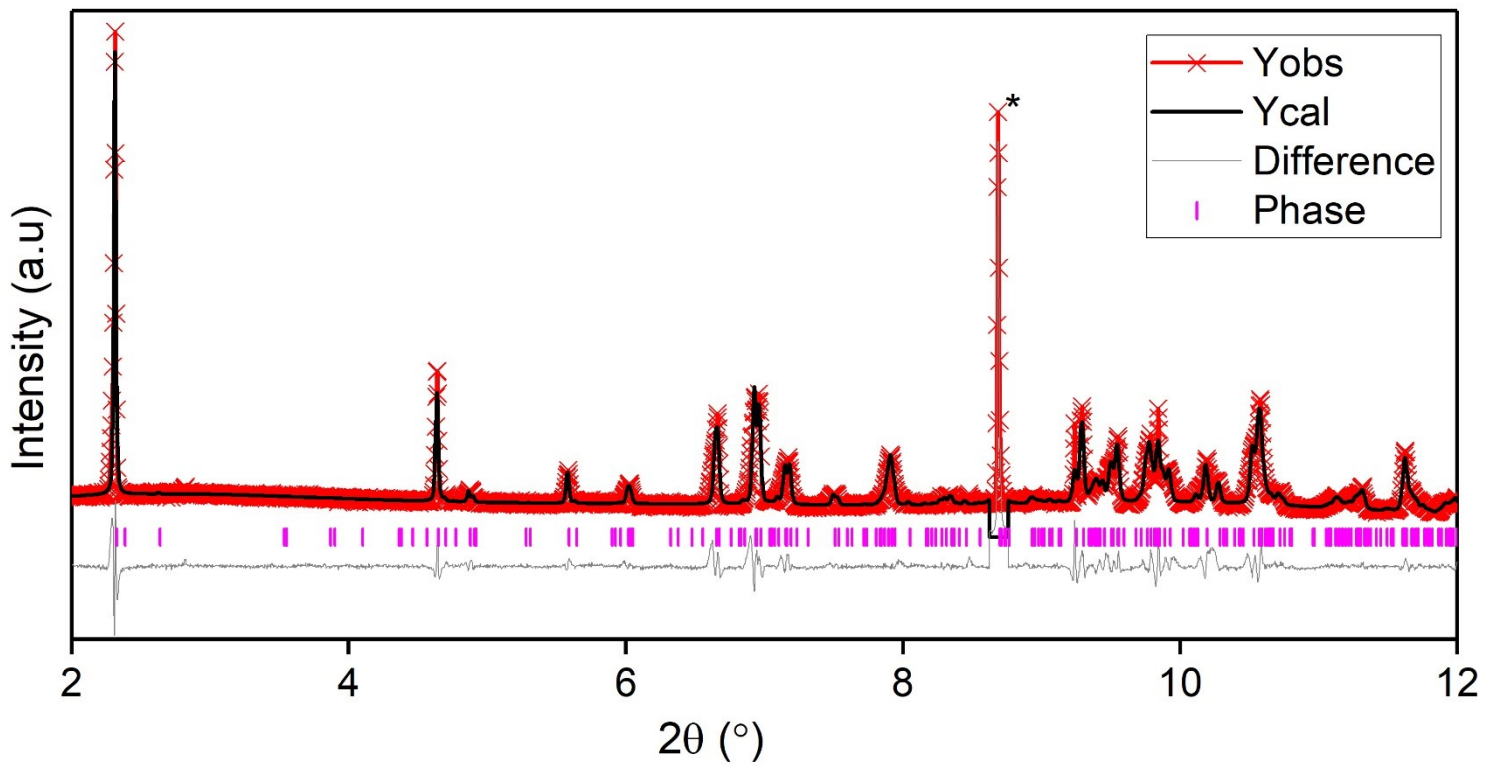


Figure S12. Le Bail refinement of PXRD pattern of $[Fe_3(N\text{-}cintrz})_6(Pd(CN)_4)_3]\cdot 6H_2O$ at 100 K. Refined parameters: $a = 10.162 \text{ \AA}$, $b = 15.716 \text{ \AA}$ and $c = 15.954 \text{ \AA}$, $\alpha = 109.680^\circ$, $\beta = 106.824^\circ$, $\gamma = 93.660^\circ$, $V = 2259.4 \text{ \AA}^3$ (*cf.* single crystal at 150 K: $a = 10.160$, $b = 15.719$, $c = 15.908$, $\alpha = 110.052^\circ$, $\beta = 106.996^\circ$, $\gamma = 93.533^\circ$, $V = 2245.2 \text{ \AA}^3$). * mark indicates the solvent freezing peak

Figure S13. Peak evolution of $[\text{Fe}_3(\text{N}-\text{cntrz})_6(\text{Pd}(\text{CN})_4)_3] \cdot 6\text{H}_2\text{O}$ over the temperature range 280–100–280 K showing the spin crossover transition.

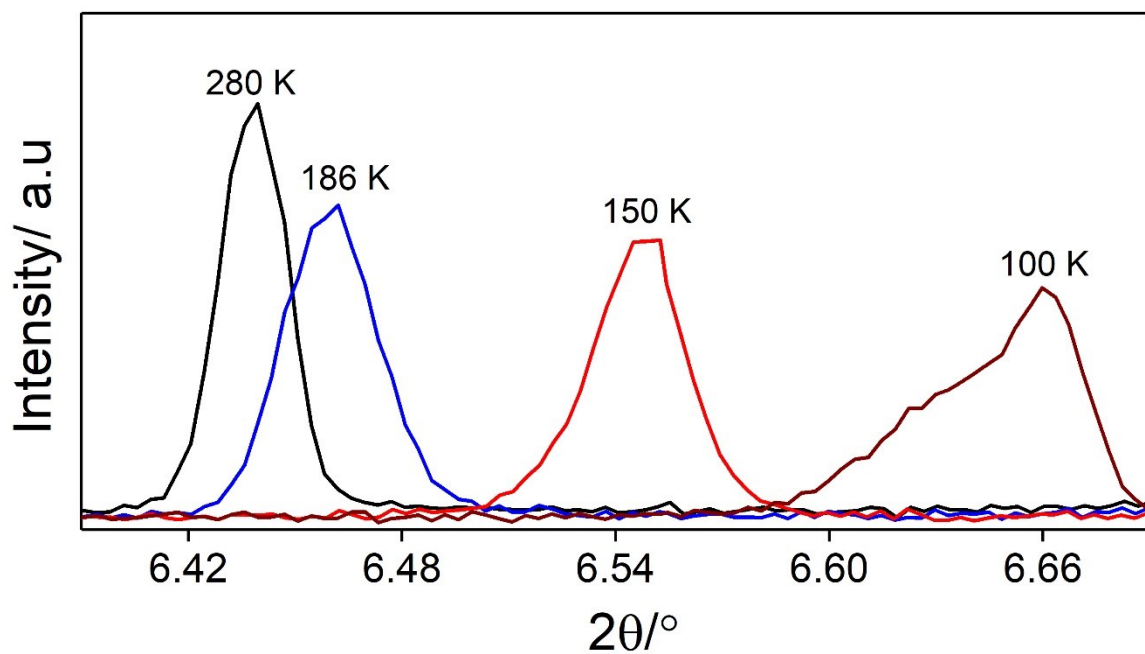
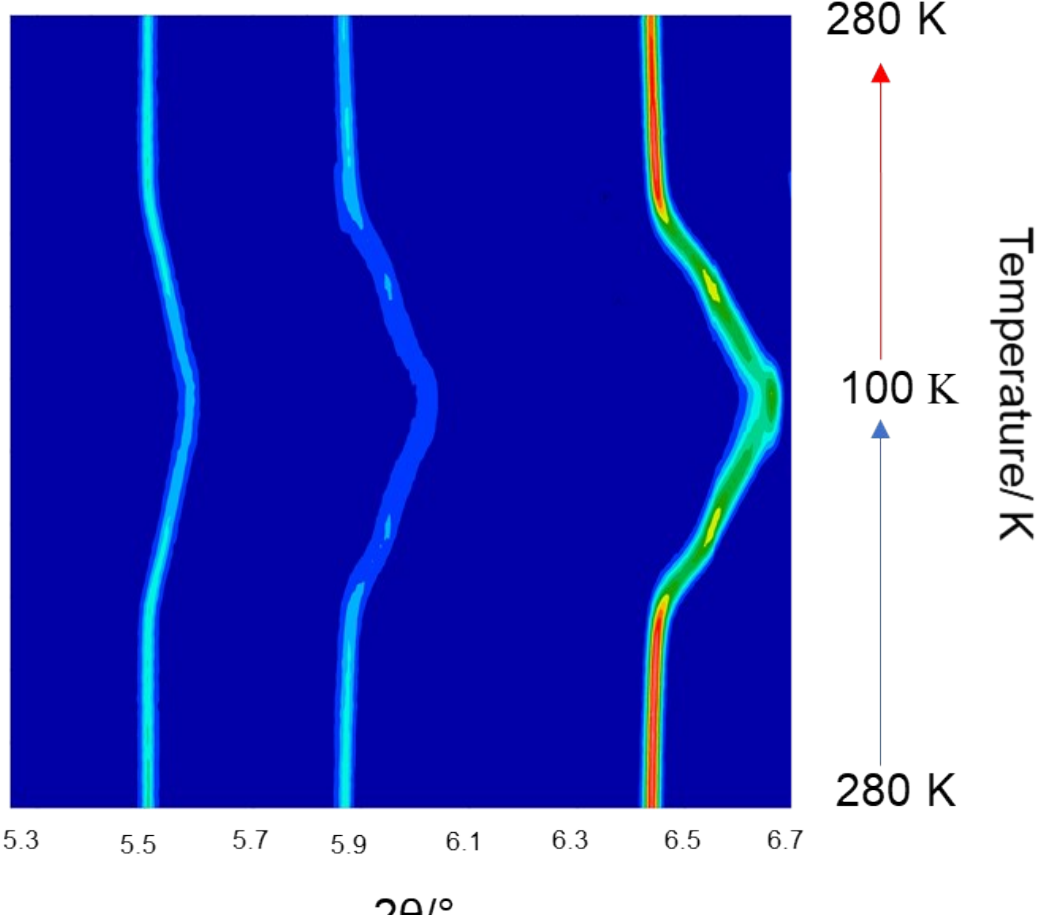


Figure S14. Comparison of the $(20-1)$ reflection at the HS plateau (280 K, black), the $\sim T_{1/2}$ (186 K, blue), the \sim intermediate plateau (150 K, red) and the \sim LS plateau (100 K, brown), highlighting the peak broadening and peak shape change with SCO.